

Continuum excitations in a spin-supersolid on a triangular lattice

M. Zhu,¹ V. Romerio,¹ N. Steiger,¹ N. Murai,² S. Ohira-Kawamura,² K. Yu. Povarov,³
Y. Skourski,³ R. Sibille,⁴ L. Keller,⁴ Z. Yan,¹ S. Gvasaliya,¹ and A. Zheludev^{1,*}

¹Laboratory for Solid State Physics, ETH Zürich, 8093 Zürich, Switzerland

²J-PARC Center, Japan Atomic Energy Agency, Tokai, Ibaraki 319-1195, Japan

³Dresden High Magnetic Field Laboratory (HLD-EMFL) and Würzburg-Dresden Cluster of Excellence *ct.qmat*,
Helmholtz-Zentrum Dresden-Rossendorf, 01328 Dresden, Germany

⁴Laboratory for Neutron Scattering and Imaging,
Paul Scherrer Institute, CH-5232 Villigen, Switzerland

(Dated: January 31, 2024)

Magnetic, thermodynamic, neutron diffraction and inelastic neutron scattering are used to study spin correlations in the easy-axis XXZ triangular lattice magnet $\text{K}_2\text{Co}(\text{SeO}_3)_2$. Despite the presence of quasi-2D “supersolid” magnetic order, the low-energy excitation spectrum contains no sharp modes and is instead a broad continuum resembling that of deconfined fractional excitations. Applying a weak magnetic field drives the system into an $m = 1/3$ fractional magnetization plateau phase where the excitations are sharp spin waves.

The Ising antiferromagnet (AF) on a triangular lattice is the textbook example of geometric frustration [1, 2]. The ubiquitous cartoon shows one spin pointing up, its neighbor pointing down to minimize exchange energy, this configuration leaving the preferred directions for their two other neighbors undefined (often illustrated as a question mark). Beyond this simplistic picture, the problem is actually a very complex one. The quantum $S = 1/2$ nearest-neighbor XXZ-model with easy-axis anisotropy is predicted to have a non-collinear ground state that can be viewed as a $\sqrt{3} \times \sqrt{3}$ “spin-supersolid” [3–5], and a series of quantum phases in applied fields. The latter include a collinear “up-up-down” (*uud*) “spin-supersolid” state corresponding that is an $m = 1/3$ magnetization plateau. Not much is known about excitations in that model, even as significant progress has recently been made in understanding its *easy plane* counterpart. There, despite the presence of long range order, the excitations are nothing like those predicted by semiclassical spin wave theory (SWT) [6]. Instead, they are dominated by bound states and continua of partially-free fractional excitations known as spinons [7]. This is taken as a fingerprint of proximate quantum spin-liquid states first hypothesized by Anderson [8, 9] and later found in numerous triangular-lattice models (see, for instance, Refs. 10–12). Does the *easy-axis* triangular AF feature similarly exotic spin dynamics?

We address this question experimentally, by thermodynamic, neutron diffraction, and inelastic neutron scattering experiments on the quasi-two-dimensional XXZ Ising-like antiferromagnet $\text{K}_2\text{Co}(\text{SeO}_3)_2$ [13]. We show that in zero field and low temperatures the system has two-dimensional magnetic order consistent with a spin-supersolid 3-sublattice structure. The low-energy spin excitation spectrum, however, is entirely dominated by a broad gapless spinon-like continuum, rather than by sharp spin wave modes. Applying a very modest external magnetic field induces a quantum critical point. Beyond

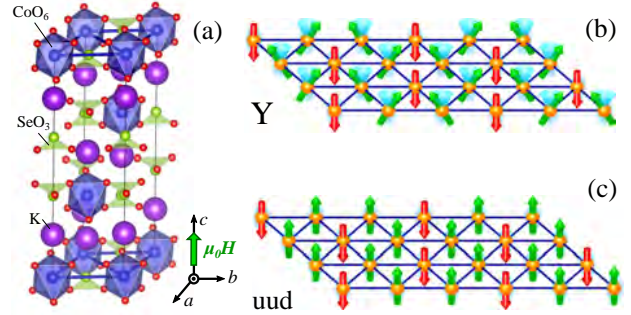


FIG. 1. (a) Schematic view of the crystal structure of $\text{K}_2\text{Co}(\text{SeO}_3)_2$. (b) The “Y” spin-supersolid phase predicted to be the ground state of an easy-axis XXZ triangular-lattice antiferromagnet. The cyan cones symbolize rotational degeneracy. (c) A magnetic field applied along the c axis stabilized a collinear “*uud*” spin-solid phase.

that the material enters an $m = 1/3$ *uud* magnetization plateau. The spectrum is drastically reconstructed. It consists of sharp gapped excitations that are perfectly reproduced by SWT.

The first magnetic studies of our target material $\text{K}_2\text{Co}(\text{SeO}_3)_2$ have been reported only recently [13]. In the layered hexagonal structure (space group $R\bar{3}m$, $a = 5.52 \text{ \AA}$, $c = 18.52 \text{ \AA}$ [14]) the key features are ABC-stacked triangular planes of Co^{2+} ions, as illustrated in Fig. 1a. As in the structurally related $\text{Na}_2\text{BaCo}(\text{PO}_4)_2$ [5, 15], the local crystallographic environment is close to octahedral, ensuring a $J = \pm 1/2$ doublet single-ion ground state. The Co^{2+} moments can be treated as $S = 1/2$ pseudospins. The shortest distance and presumably the strongest magnetic interaction is between nearest-neighbor ions in each plane. Previous magnetometric studies have confirmed the dominance of AF coupling with very strong easy-axis type anisotropy [13]. In zero applied field the system seems to avoid any magnetic

ordering down to 0.35 K. Only a broad bump is observed in specific heat at around $T \sim 1$ K, perhaps indicating short range order. In contrast, in magnetic fields exceeding 1 T directed along the c axis, a sharp specific heat anomaly indicates robust long-range ordering at temperatures as high as 11 K at 9 T. It was initially suggested that this behavior corresponds to a metamagnetic transition to a fully polarized state.

The first significant finding of the present study is that the magnetic state above 1 T is *not* a fully polarized one, but an $m = 1/3$ magnetization plateau. This is obvious from the magnetization curves measured at $T = 1.3$ K on a 5.4 mg single crystal sample by the coaxial pick-up coil pulsed-field magnetometer at HLD-EMFL [16], and plotted in Fig. 2a. As in all experiments reported below the field is applied along the crystallographic c -axis (magnetic easy axis). Note that full saturation is reached only at $\mu_0 H_{\text{sat}} \approx 22$ T. The difference between the up-sweep and down-sweep curves is instrumental and due to magnetocaloric effect. A more detailed field-temperature magnetic phase diagram of $\text{K}_2\text{Co}(\text{SeO}_3)_2$ was established in calorimetric experiments. These were performed on a Quantum Design PPMS with a dilution refrigerator insert using a 0.05 mg single crystal sample. The result is presented in a false color C/T specific heat plot in Fig. 2b, with some selected temperature scans shown in Supplemental Material. The sharp high-temperature/high-field lambda-anomaly reported in [13] is also visible in our data. This well-defined phase boundary has a well-defined endpoint at $(\mu_0 H_0 \approx 1.05$ T, $T_0 \approx 4.5$ K), indicated by a yellow diamond. At lower field this anomaly is absent. Instead there is a broad crossover line (dashed) that extends down to zero field and corresponds to the bump at $T \sim 1$ K. An unexpected finding is an additional low-temperature phase boundary marked by a somewhat rounded specific heat maxima (see Supplement). It has the shape of a “dome” of some magnetically ordered phase with a zero-field ordering temperature $T_c \approx 0.35$ K, and terminates in a quantum critical point $\mu_0 H_c = 0.8$ T. Overall, the phase diagram is qualitatively similar to that theoretically predicted for the triangular easy-axis system $\text{Na}_2\text{BaCo}(\text{PO}_4)_2$ [5].

To better understand the observed behavior, we performed neutron diffraction experiments at the DMC powder instrument and ZEBRA lifting-counter diffractometer at Paul Scherrer Institut, as well as the AMATERAS time of flight (TOF) spectrometer at J-PARC [17]. In the latter two experiments we utilized 75 and 425 mg single crystal samples, respectively. Sample environment was a ^3He - ^4He dilution refrigerator on AMATERAS and a standard ^4He cryostat on ZEBRA. In both cases a cryomagnet was used to produce a magnetic field along the c axis. Elastic scattering intensity measured at $T = 70$ mK in zero field in the $(h, k, 0)$ plane using the TOF technique with $E_i = 7.73$ meV incident-energy neutrons is shown in Fig. 3a. A practically identical diffraction pat-

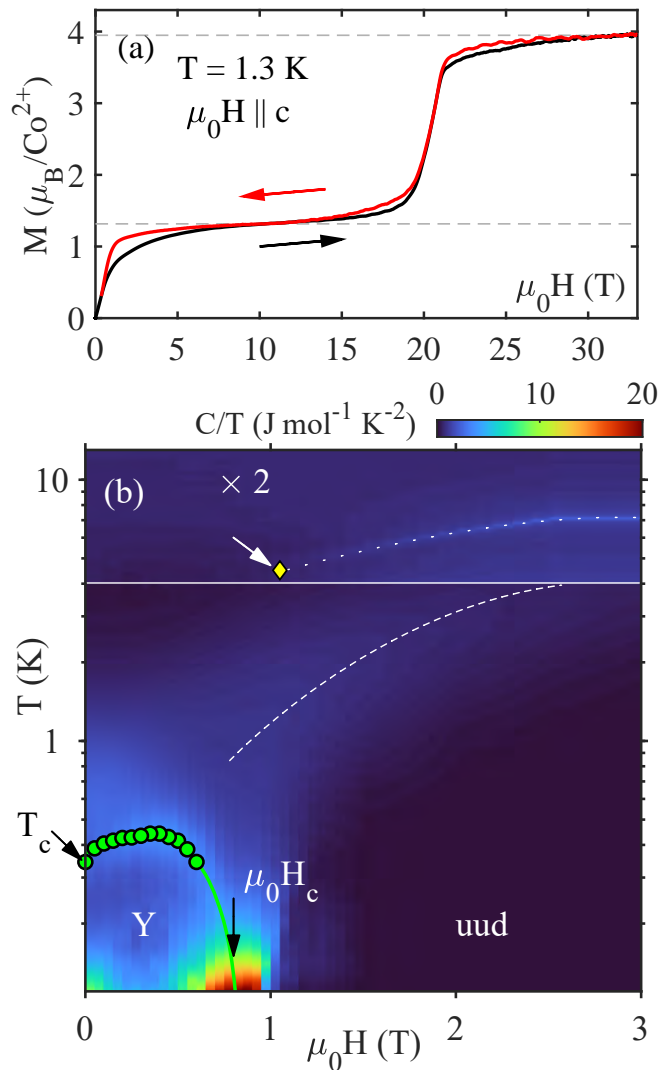


FIG. 2. (a) Magnetization curves measured in $\text{K}_2\text{Co}(\text{SeO}_3)_2$ in a pulsed magnetic field applied along the crystallographic c axis. The difference between up- and down-sweeps is due to magnetocaloric effect. Dashed lines indicate full and $1/3$ pseudospin polarization. (b) False-color plot of specific heat C/T measured as a function of temperature (note the logarithmic axis scale) and field in the same geometry. The sharp high-temperature lambda anomaly (dotted line) discussed in [13] has an endpoint (diamond). The dashed line is a broad crossover. The solid line encloses a phase pocket with an ordering temperature T_c . At $T \rightarrow 0$ there is a quantum critical point at H_c . Circles indicate the positions of local specific heat maxima in temperature scans measured at a constant field.

tern is seen in a $\mu_0 H = 1.5$ T field (see Supplement). Both demonstrate magnetic Bragg scattering indexed by a $(1/3, 1/3)$ 2D propagation vector (arrows). This corresponds to a $\sqrt{3} \times \sqrt{3}$ magnetic unit cell in the triangular plane. In zero field this scattering sets in without any apparent phase transition (Fig. 3c, ZEBRA data), and simply increases steadily upon cooling below about 10 K.

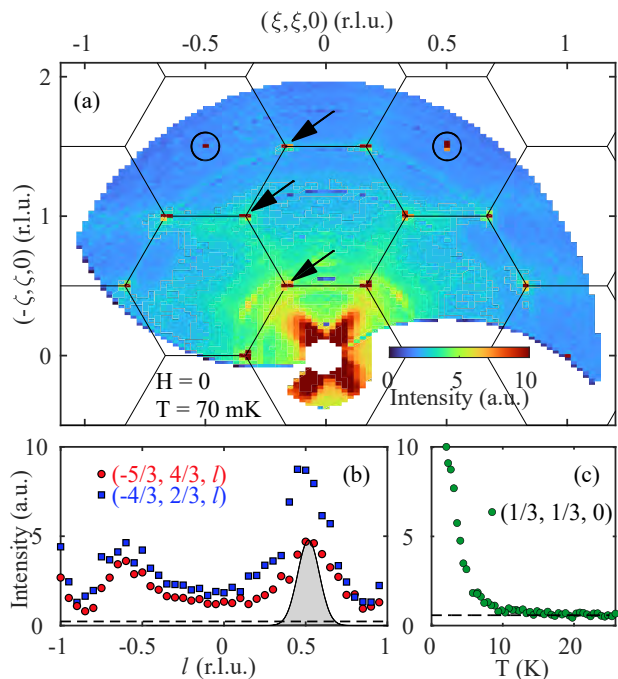


FIG. 3. Elastic scattering measured in $\text{K}_2\text{Co}(\text{SeO}_3)_2$ in zero field. (a) TOF data collected at $T = 70$ mK in the $(h, k, 0)$ plane reveal $(1/3, 1/3)$ -type two-dimensional order (arrows). Circles highlight allowed structural Bragg peaks. Solid lines are 2D Brillouin zone boundaries for a single triangular plane. (b) Cuts from the same data set along the l direction show only short-range correlations between planes. The shaded Gaussian represent the measured experimental Bragg wave vector resolution. (c) Temperature dependence of diffraction intensity at the $(1/3, 1/3, 0)$ position using a single-detector diffractometer. In all cases the dashed lines are the background level measured just off the corresponding $(1/3, 1/3)$ position. Error bars are smaller than symbol size.

At higher fields it follows a more typical order-parameter like curve with a transition exactly corresponding to the specific heat lambda-anomaly (see Supplement).

In all measurements the magnetic elastic scattering is resolution-limited in the h and k . At the same time, it represents 2D, rather than 3D order. This can be seen in Fig. 3b, which show scans along the $(-5/3, 4/3, l)$ and $(-4/3, 2/3, l)$ Bragg-rods. Far from being a resolution-limited Bragg peak, as a function of l , the signal is only weakly modulated. This is also the case in applied fields (see Supplement). Thus, we are dealing with the physics of single magnetic planes and only very short-range inter-plane correlations.

Due to the rather complex out-of-plane modulation, possible magnetic domains and the fact that the uud and supersolid phases share the same propagation vector, a determination of the exact 2D magnetic structures from the available data does not appear feasible. Instead, we can seek some guidance from theory. The ground state of the *classical* XXZ easy-axis antiferro-

magnet on a triangular lattice is a 3-sublattice planar “Y” structure [2], as shown in Fig. 1b. All spins on one sublattice are pointing “down”. On the two other sublattices they are canted away from the “up” direction forming an angle $\phi < 2\pi/3$ between them. In the isotropic limit $\phi \rightarrow 2\pi/3$ this is the famous “120°” structure of the Heisenberg model. The Y-state is a commensurate spin density wave for the z -components with a $\sqrt{3} \times \sqrt{3}$ unit cell, the “down” being arranged in a honeycomb geometry. It thereby breaks a \mathbb{Z}_3 discrete translation symmetry. The breaking of both these discrete symmetries in 2D can be expected to survive at finite temperatures. Crucially, the in-plane spin components of the Y-structure also breaks continuous $SO(2)$ rotational symmetry around the z axis. As in the XY model, the transverse components will show at most quasi-long-range order at a finite temperature, and may eventually undergo a Berezinskii–Kosterlitz–Thouless (BKT) type transition [18]. Another consequence of broken continuous symmetry is a gapless spectrum.

In applied fields theory predicts a transition to the collinear uud plateau phase illustrated in Fig. 1c. This structure breaks only discrete symmetries and may thus persist at finite temperatures. The magnetic excitation spectrum is gapped. Upon decreasing the field, the transition to the Y-phase occurs when the lowest gapped magnon softens at some critical field H_c . As realized by Batyev and Braginski sense [19] this transition is mapped on a Bose-Einstein condensation (BEC) of magnons. Since it occurs in a “spin-solid” state with spontaneously broken translation symmetry, the low-field state is a “spin supersolid” in the Andreev sense [20, 21].

For quantum spins the situation is qualitatively similar. The phase boundaries are shifted compared to those in the classical model, and all spins are subject to quantum fluctuations and a corresponding reduction of the order parameter [3, 4]. This prompts us to hypothesize the following picture, that in many ways echoes the behavior predicted theoretically for $\text{Na}_2\text{BaCo}(\text{PO}_4)_2$ [5]. The robust $(1/3, 1/3)$ 2D magnetic correlations observed experimentally in $\text{K}_2\text{Co}(\text{SeO}_3)_2$ are primarily due to the z components of spins, which are similarly ordered in both uud - and Y-phases. They form already at $T \gg T_c$ and represent the spin solid. In zero field T_c then corresponds to long-range or BKT ordering of the transverse spin components, resulting in a compressible spin-supersolid with a gapless spectrum. A BEC-type solid-supersolid quantum phase transition occurs at H_c . The main differences with the theory on $\text{Na}_2\text{BaCo}(\text{PO}_4)_2$ are the presence of the end-point at (H_0, T_0) in $\text{K}_2\text{Co}(\text{SeO}_3)_2$, a much wider plateau, and a much higher saturation field.

The emerging picture is fully consistent with the main result of the present study, namely measurements of the magnetic excitations. In Fig. 4a-c we show false-color neutron intensity plots of energy-momentum cuts through the data collected at the AMATERAS spec-

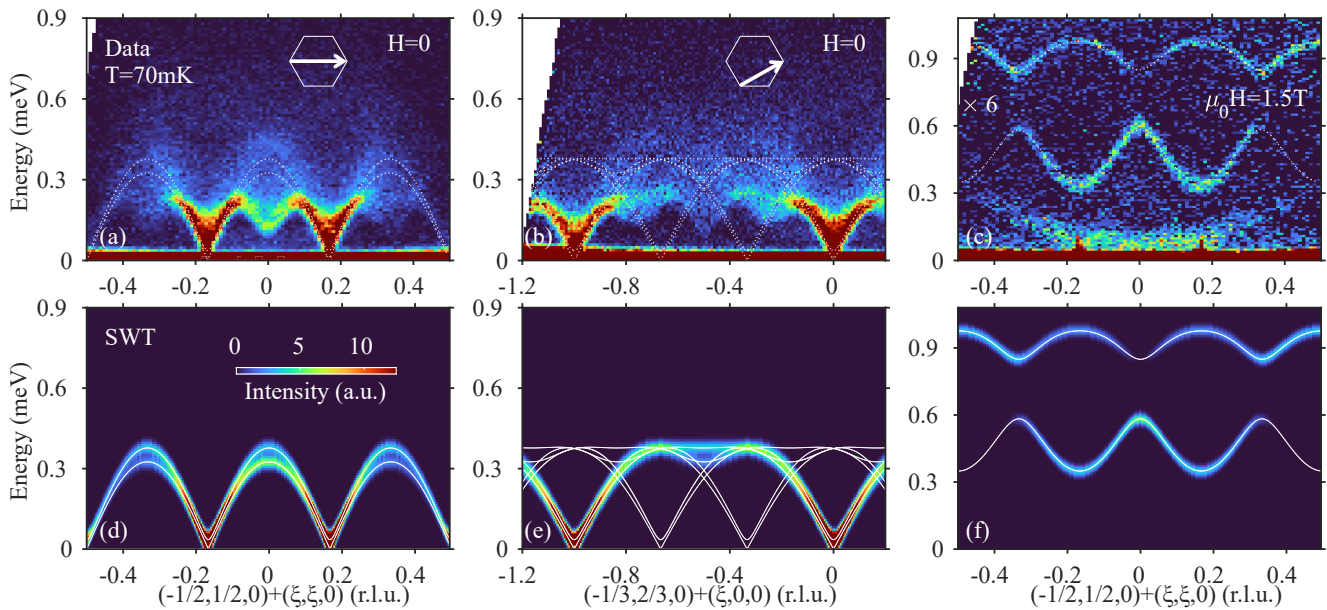


FIG. 4. False-color plots of inelastic neutron intensity measured in $\text{K}_2\text{Co}(\text{SeO}_3)_2$ at $T = 70$ mK in zero field (a and b), and in $\mu_0 H = 1.5$ T applied along the c axis (c). The inset shows the direction of the cut relative to the Brillouin zone of the triangular lattice. In the latter, note the $\times 6$ scale factor. The data were integrated along the l axis in the entire range, and within ± 0.1 r.l.u. along the transverse direction within the $(0, 0, 1)$ -plane. No background is subtracted. The low-energy scattering in (c) is spurious, originating from the sample environment. It is also present in (a) but not visible due to a different color range. (d-f) as well as white lines in all panels show corresponding simulations based on linear spin wave theory, as described in the text.

trometer using $E_i = 2.24$ meV neutrons. These data were integrated in the entire accessible l -range and within ± 0.1 r.l.u. in the $(h, k, 0)$ plane perpendicular to the cut. Fig. 4a,b are cuts along the $(-1/2, 1/2, 0) + (\xi, \xi, 0)$ and $(-1/3, 2/3, 0) + (\xi, 0, 0)$ reciprocal-space lines, respectively, measured in zero field. Fig. 4c is the same cut as in (a), but measured at $\mu_0 H = 1.5$ T. The difference between zero field and 1.5 T data could hardly be more vivid. In the former case excitations are gapless. The spectrum is a broad continuum with no coherent modes, reminiscent of multi-spinon continua in quantum spin chains [22]. In contrast, at 1.5 T the excitations are all sharp and in fact resolution limited.

The contrast is made even more obvious if we compare the observations with linear SWT calculations. We based these on a simple nearest-neighbor exchange model with just three parameters: the g -factor for the effective $S = 1/2$ pseudospin, and the exchange constants J_{zz} and J_{xy} , for the out-of-plane and in-plane spin components, correspondingly. All simulations were performed using the SPIN-W software package [23]. First, we used simplistic Gaussian fits to the data in order to quantify the measured dispersion relation in the uud phase. The result was then fit to linear spin wave theory to obtain $g = 8.34(6)$, $J_{zz} = 0.68(6)$ meV and $J_{xy} = 0.25(1)$ meV. The dispersion relation computed with these values is shown in white lines in Fig. 4a-c. The corresponding intensity simulations are shown in Fig. 4d-f [24] Here we

have assumed a Gaussian energy broadening that corresponds to the actual experimental resolution of the 2.24 meV AMATERAS setup.

For $\mu_0 H = 1.5$ T SWT reproduces the experimental data up to 1 meV transfer exceptionally well. As discussed in the Supplement, it also predicts a 3rd mode at a higher energy, one is not seen in the measurement. In contrast, in zero field the computed low-energy spectra are drastically different from what is actually observed, and not only in what concerns excitation widths. For spinon continua in Heisenberg spin chains [25], the computed shape of the SWT dispersion qualitatively resembles the lower bound of the continuum. Quite to the opposite, in $\text{K}_2\text{Co}(\text{SeO}_3)_2$ the latter has a distinct dip at the $(1/2, 1/2)$ zone-boundary, not captured by SWT. Similar “roton-like minima” were observed in the easy-plane case [6] as well.

We are at present unaware of a suitable theoretical framework to describe the continuum seen in zero field. As discussed above, these gapless excitations must be related to the in-plane spin components in the spin-solid phase. These degrees of freedom are somewhat similar to the ordered moment in an easy-plane system. One may be tempted to draw direct analogies with spinon continua in the planar XXZ triangular model [6, 7] or distorted triangular-lattice systems [26–28], but that is not quite justified. Indeed, in the ground state of the axial model these degrees of freedom live on a hexagonal,

rather than triangular lattice. Thus, further theoretical work is needed to understand the observed continua.

In summary, the Ising-like triangular lattice antiferromagnet $\text{K}_2\text{Co}(\text{SeO}_3)_2$, despite translation symmetry breaking long range order, demonstrates gapless continuum spin dynamics in the spin-supersolid phase. It strongly resembling that of deconfined spinons. In contrast, the field-induced spin-solid state only has coherent gapped magnons. Similarly to the case of some one-dimensional magnets [29, 30], the confinement of fractional excitations can be switched on and off simply by varying the external field and driving the system through a quantum critical point.

This work was Supported by a MINT grant of the Swiss National Science Foundation. AZ thanks Prof. A. Chernyshev (UC Irvine) for pointing out some of the literature referenced in this work. Many thanks to J. Nagl for help with graphical illustrations. We acknowledge the support of the HLD at HZDR, member of the European Magnetic Field Laboratory (EMFL), and the Würzburg-Dresden Cluster of Excellence on Complexity and Topology in Quantum Matter - ct.qmat (EXC 2147, project ID 390858490). Data at J-PARC were collected in Experiment no. 2023B0161. While preparing this manuscript, we became aware of Ref. [31] that seems to announce independent but similar findings.

* zhelud@ethz.ch; <http://www.neutron.ethz.ch/>

- [1] G. H. Wannier, Antiferromagnetism. the triangular ising net, *Phys. Rev.* **79**, 357 (1950).
- [2] S. Miyashita, Magnetic properties of ising-like heisenberg antiferromagnets on the triangular lattice, *Journal of the Physical Society of Japan* **55**, 3605 (1986), <https://doi.org/10.1143/JPSJ.55.3605>.
- [3] D. Heidarian and A. Paramekanti, Supersolidity in the triangular lattice spin-1/2 xxz model: A variational perspective, *Phys. Rev. Lett.* **104**, 015301 (2010).
- [4] D. Yamamoto, G. Marmorini, and I. Danshita, Quantum phase diagram of the triangular-lattice xxz model in a magnetic field, *Phys. Rev. Lett.* **112**, 127203 (2014).
- [5] Y. Gao, Y.-C. Fan, H. Li, F. Yang, X.-T. Zeng, X.-L. Sheng, R. Zhong, Y. Qi, Y. Wan, and W. Li, Spin supersolidity in nearly ideal easy-axis triangular quantum antiferromagnet $\text{Na}_2\text{BaCo}(\text{PO}_4)_2$, *npj Quantum Materials* **7**, 89 (2022).
- [6] D. Macdougall, S. Williams, D. Prabhakaran, R. I. Bewley, D. J. Voneshen, and R. Coldea, Avoided quasiparticle decay and enhanced excitation continuum in the spin- $\frac{1}{2}$ near-heisenberg triangular antiferromagnet $\text{Ba}_3\text{CoSb}_2\text{O}_9$, *Phys. Rev. B* **102**, 064421 (2020).
- [7] E. A. Ghioldi, S.-S. Zhang, Y. Kamiya, L. O. Manuel, A. E. Trumper, and C. D. Batista, Evidence of two-spinon bound states in the magnetic spectrum of $\text{Ba}_3\text{CoSb}_2\text{O}_9$, *Phys. Rev. B* **106**, 064418 (2022).
- [8] P. Anderson, Resonating valence bonds: A new kind of insulator?, *Materials Research Bulletin* **8**, 153 (1973).
- [9] L. Balents, Spin liquids in frustrated magnets, *Nature* **464**, 199 EP (2010).
- [10] Y. Iqbal, W.-J. Hu, R. Thomale, D. Poilblanc, and F. Becca, Spin liquid nature in the heisenberg $J_1 - J_2$ triangular antiferromagnet, *Phys. Rev. B* **93**, 144411 (2016).
- [11] A. Wietek and A. M. Läuchli, Chiral spin liquid and quantum criticality in extended $s = \frac{1}{2}$ heisenberg models on the triangular lattice, *Phys. Rev. B* **95**, 035141 (2017).
- [12] S. Hu, W. Zhu, S. Eggert, and Y.-C. He, Dirac spin liquid on the spin-1/2 triangular heisenberg antiferromagnet, *Phys. Rev. Lett.* **123**, 207203 (2019).
- [13] R. Zhong, S. Guo, and R. J. Cava, Frustrated magnetism in the layered triangular lattice materials $\text{K}_2\text{Co}(\text{SeO}_3)_2$ and $\text{Rb}_2\text{Co}(\text{SeO}_3)_2$, *Phys. Rev. Mater.* **4**, 084406 (2020).
- [14] M. Wildner, Isotypism of a selenite with a carbonate: structure of the buetschliite-type compound $\text{K}_2\text{Co}(\text{SeO}_3)_2$, *Acta Crystallographica Section C* **48**, 410 (1992).
- [15] C. Wellm, W. Roscher, J. Zeisner, A. Alfonsov, R. Zhong, R. J. Cava, A. Savoyant, R. Hayn, J. van den Brink, B. Büchner, O. Janson, and V. Kataev, Frustration enhanced by Kitaev exchange in a $\tilde{J}_{\text{eff}} = \frac{1}{2}$ triangular antiferromagnet, *Phys. Rev. B* **104**, L100420 (2021).
- [16] Y. Skourski, M. D. Kuz'min, K. P. Skokov, A. V. Andreev, and J. Wosnitzer, High-field magnetization of $\text{ho}_2\text{fe}_{17}$, *Phys. Rev. B* **83**, 214420 (2011).
- [17] K. Nakajima, S. Ohira-Kawamura, T. Kikuchi, M. Nakamura, R. Kajimoto, Y. Inamura, N. Takahashi, K. Aizawa, K. Suzuya, K. Shibata, T. Nakatani, K. Soyama, R. Maruyama, H. Tanaka, W. Kambara, T. Iwahashi, Y. Itoh, T. Osakabe, S. Wakimoto, K. Kakurai, F. Maekawa, M. Harada, K. Oikawa, R. E. Lechner, F. Mezei, and M. Arai, Amateras: A cold-neutron disk chopper spectrometer, *Journal of the Physical Society of Japan* **80**, SB028 (2011).
- [18] J. M. Kosterlitz and D. J. Thouless, Ordering, metastability and phase transitions in two-dimensional systems, *Journal of Physics C: Solid State Physics* **6**, 1181 (1973).
- [19] E. G. Batyev and L. S. Braginski, *Sov. Phys. JETP* **60**, 781 (1984).
- [20] A. F. Andreev and I. M. Lifshitz, Quantum theory of defects in crystals, *Soviet Physics Uspekhi* **13**, 670 (1971).
- [21] O. A. Starykh, Unusual ordered phases of highly frustrated magnets: a review, *Rep. Prog. Phys.* **78**, 052502 (2015).
- [22] M. B. Stone, D. H. Reich, C. Broholm, K. Lefmann, C. Rischel, C. P. Landee, and M. M. Turnbull, Extended Quantum Critical Phase in a Magnetized Spin-12 Antiferromagnetic Chain, *Phys. Rev. Lett.* **91**, 037205 (2003).
- [23] S. Toth and B. Lake, Linear spin wave theory for single- Q incommensurate magnetic structures, *J. Phys.: Condens. Matter* **27**, 166002 (2015).
- [24] Due to the classical degeneracy in zero applied field, the Y -structure is not a unique classical ground state. In order to perform an SWT calculation for $H \rightarrow 0$, we assumed a tiny $H = 30$ G field along the c axis. This uniquely selects the Y structure as the ground state but opens a gap $\Delta \sim 0.04$ meV in one of the spin wave branches. This artificially-induced residual gap is apparent in all zero-field simulations near the magnetic Bragg points.
- [25] G. Müller, H. Thomas, H. Beck, and J. C. Bonner, Quantum spin dynamics of the antiferromagnetic linear chain in zero and nonzero magnetic field, *Phys. Rev. B* **24**, 1429

- (1981).
- [26] R. Coldea, D. A. Tennant, and Z. Tylczynski, Extended scattering continua characteristic of spin fractionalization in the two-dimensional frustrated quantum magnet Cs_2CuCl_4 observed by neutron scattering, *Phys. Rev. B* **68**, 134424 (2003).
- [27] M. Kohno, O. A. Starykh, and L. Balents, Spinons and triplons in spatially anisotropic frustrated antiferromagnets, *Nat. Physics* **3**, 790 (2007).
- [28] K. Nawa, D. Hirai, M. Kofu, K. Nakajima, R. Murasaki, S. Kogane, M. Kimata, H. Nojiri, Z. Hiroi, and T. J. Sato, Bound spinon excitations in the spin- $\frac{1}{2}$ anisotropic triangular antiferromagnet $\text{Ca}_3\text{ReO}_5\text{Cl}_2$, *Phys. Rev. Research* **2**, 043121 (2020).
- [29] M. Mourigal, M. Enderle, A. Klöpperpieper, J.-S. Caux, A. Stunault, and H. M. Rønnow, Fractional spinon excitations in the quantum Heisenberg antiferromagnetic chain, *Nat. Phys.* **9**, 435 (2013).
- [30] D. Schmidiger, P. Bouillot, T. Guidi, R. Bewley, C. Kollath, T. Giamarchi, and A. Zheludev, Spectrum of a Magnetized Strong-Leg Quantum Spin Ladder, *Phys. Rev. Lett.* **111**, 107202 (2013).
- [31] A. Ghasemi, T. Chen, J. Zhang, L. Shi, E.-S. Choi, M. Lee, Y. Hao, H. Cao, B. Winn, M. Jaime, X. Xu, R. Zhong, R. Cava, P. Armitage, and C. Broholm, Quantum fluctuations in an easy axis spin-1/2 triangular lattice antiferromagnet. APS March Meeting 2024, Abstract no. Y23.00007.

Continuum excitations in a spin-supersolid on a triangular lattice: Supplementary material

M. Zhu,¹ V. Romerio,¹ N. Steiger,¹ N. Murai,² S. Ohira-Kawamura,² K. Yu. Povarov,³
Y. Skourski,³ R. Sibille,⁴ L. Keller,⁴ Z. Yan,¹ S. Gvasaliya,¹ and A. Zheludev^{1,*}

¹Laboratory for Solid State Physics, ETH Zürich, 8093 Zürich, Switzerland

²J-PARC Center, Japan Atomic Energy Agency, Tokai, Ibaraki 319-1195, Japan

³Dresden High Magnetic Field Laboratory (HLD-EMFL) and Würzburg-Dresden Cluster of Excellence *ct.qmat*,
Helmholtz-Zentrum Dresden-Rossendorf, 01328 Dresden, Germany

⁴Laboratory for Neutron Scattering and Imaging,
Paul Scherrer Institute, CH-5232 Villigen, Switzerland

(Dated: January 31, 2024)

CALORIMETRY DATA

The false-color specific heat plot shown in Fig. 2b in the main text combines a series of constant-field temperature scans. Typical low-temperature data are shown in Fig. S1.

DIFFRACTION IN APPLIED FIELDS

Diffraction data collected on AMATERAS at $\mu_0 H = 1.5$ T are shown in Fig. S2. They are very similar to what is seen in zero field, except for an increased overall intensity of magnetic scattering.

Unfortunately, the temperature dependence of magnetic intensity at $\mu_0 H = 1.5$ T was not measured in our ZEBRA experiment. Instead, Fig. S3 compares the gradual temperature evolution of the magnetic intensity at $(1/3, 1/3, 0)$ seen in zero fields (same data as in Fig. 3c in the main text) with clear order-parameter-like behavior deep in the *uud* phase, at $\mu_0 H = 6$ T.

HIGHER-ENERGY SPIN WAVES

In Fig. S4 we show the same data and simulations as in Fig. 4 of the main text, the only difference being a wider energy range shown. We see that SWT predicts an additional rather flat band that in all cases lies above 1 meV energy transfer. This mode is not detected in the measurement. Most striking is the case of $\mu_0 H = 1.5$ T, where SWT seems to provide a perfect fit at low

energies, yet also predicts this “extra” branch at 1.2 meV. Experimentally it is totally absent: data collected with a higher incident energy at $\mu_0 H = 1.5$ T do not show any other excitations up to 5 meV transfer.

We can only speculate that this effect is beyond the linear SWT approximation. For example, the 1.2 meV mode may be rendered unstable towards a decay into two excitations in the lowest-energy branch, similar to the effects discussed in [1]. Such a decay process would indeed be permitted by energy-momentum conservation. Since magnetic inelastic scattering intensities at $\mu_0 H = 1.5$ T are already much weaker than in zero field, even a moderate decay-induced broadening of the SWT-predicted branch would render it experimentally undetectable.

In this context, we note that there are very good grounds to rely on SWT in the fully polarized phase, where in the presence of axial symmetry it becomes exact. Even though the *uud* phase is collinear, SWT is *not* exact there. In fact, strong non-linear SWT effects have been observed in other triangular-lattice magnets in their $m = 1/3$ plateau state [2].

* zhelud@ethz.ch; <http://www.neutron.ethz.ch/>

[1] M. E. Zhitomirsky and A. L. Chernyshev, Colloquium: Spontaneous magnon decays, *Rev. Mod. Phys.* **85**, 219 (2013).

[2] Y. Kamiya, L. Ge, T. Hong, Y. Qiu, D. L. Quintero-Castro, Z. Lu, H. B. Cao, M. Matsuda, E. S. Choi, C. D. Batista, M. Mourigal, Z. H. D., and J. Ma, The nature of spin excitations in the one-third magnetization plateau phase of $\text{Ba}_3\text{CoSb}_2\text{O}_9$, *Nat. Commun.* **9**, 2666 (2018).

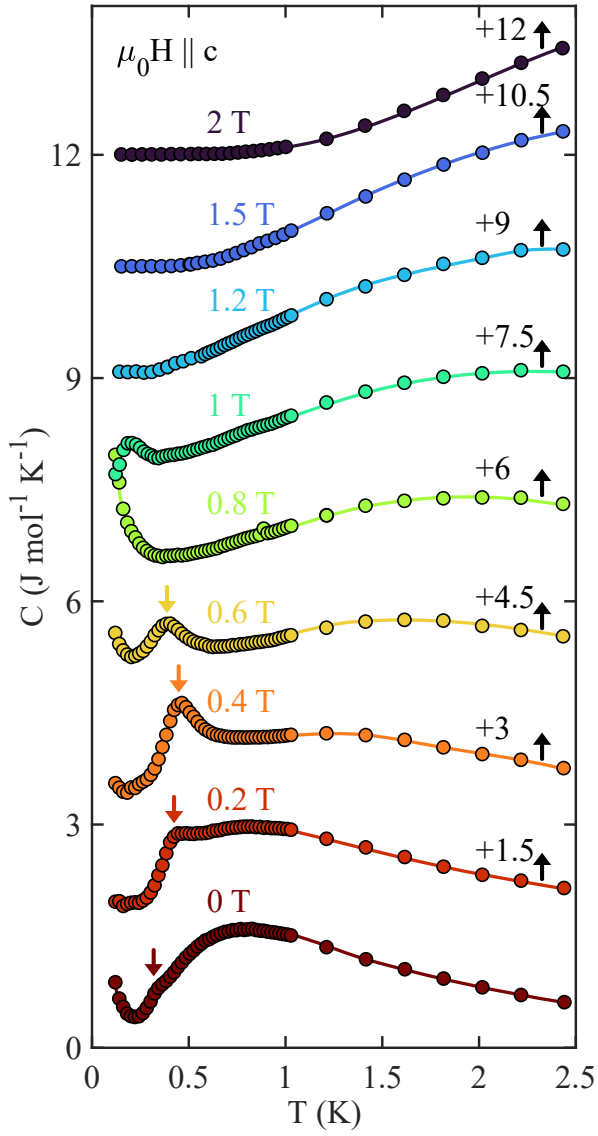


FIG. S1. Typical constant-field scans of specific heat, as measured in $\text{K}_2\text{Co}(\text{SeO}_3)_2$ using the thermal-relaxation method in different magnetic fields applied along the c axis. Individual plots are offset for visibility as indicated on the right. Arrows on the left indicate anomalies on the boundary of the low-temperature spin-solid phase.

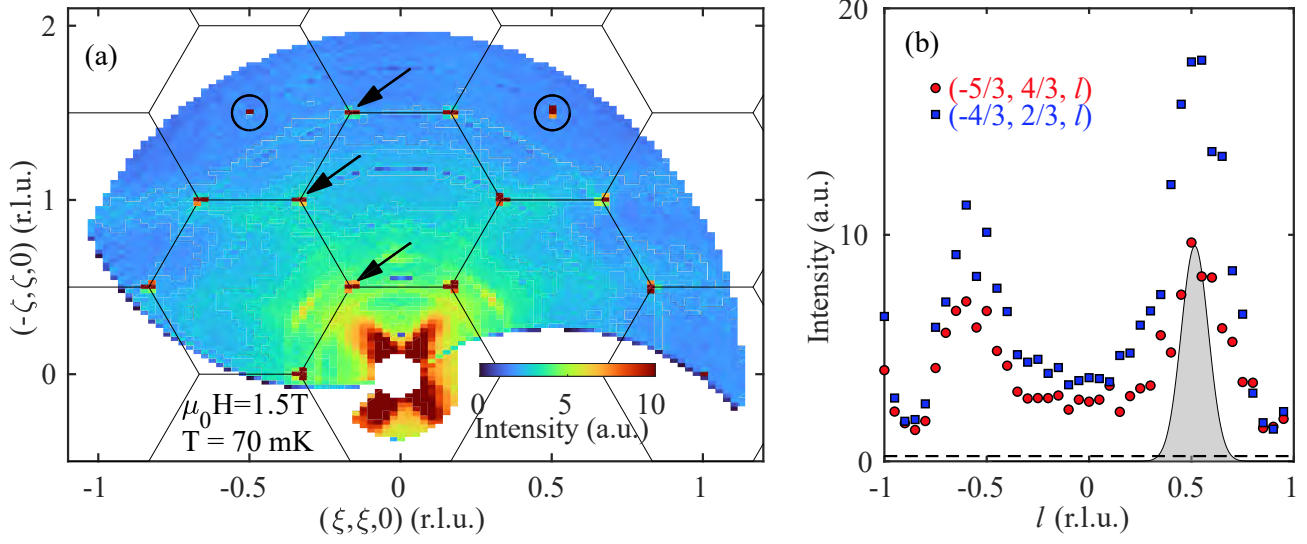


FIG. S2. Elastic scattering measured in $\text{K}_2\text{Co}(\text{SeO}_3)_2$ in a magnetic field $\mu_0 H = 1.5$ T. (a) TOF data collected at $T = 70$ mK in the $(h, k, 0)$ plane reveal $(1/3, 1/3)$ -type two-dimensional order (arrows). Circles highlight allowed structural Bragg peaks. Solid lines are 2D Brillouin zone boundaries for a single triangular plane. (b) Cuts from the same data set along the l direction show only short-range correlations between planes. The shaded Gaussian represent the measured experimental Bragg wave vector resolution. The dashed line is the background level measured just off the $(1/3, 1/3)$ position. Error bars are smaller than symbol size.

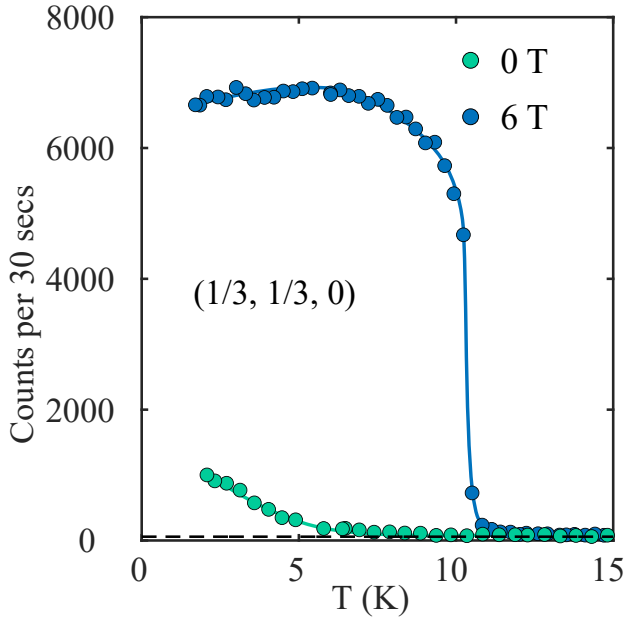


FIG. S3. Temperature dependence of neutron diffraction intensity measured at $(1/3, 1/3, 0)$ in zero field and at $\mu_0 H = 6$ T. Dashed line is the background measured slightly off the Bragg rod. Error bars are smaller than symbol size.

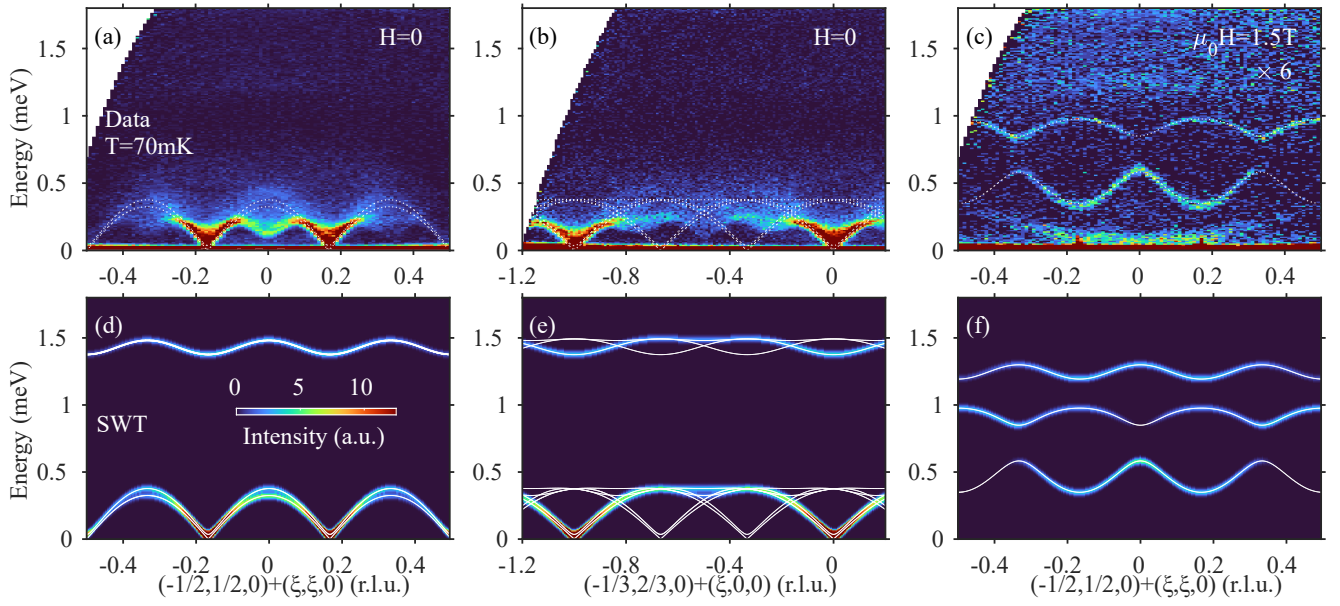


FIG. S4. False-color plots of inelastic neutron intensity measured in $\text{K}_2\text{Co}(\text{SeO}_3)_2$ at $T = 70$ mK in zero field (a and b), and in $\mu_0 H = 1.5$ T applied along the c axis (c). In the latter, note the $\times 6$ scale factor. The data were integrated along the l axis in the entire range, and within ± 0.1 r.l.u. along the transverse direction within the $(0, 0, 1)$ -plane. No background is subtracted. The low-energy scattering in (c) is spurious, originating from the sample environment. It is also present in (a) but not visible due to a different color range. (d-f) as well as white lines in all panels show corresponding simulations based on linear spin wave theory, as described in the text.